Letter

Ultrafast creation and melting of nonequilibrium excitonic condensates in bulk WSe_2

E. Perfetto and G. Stefanucci
Dipartimento di Fisica, Università di Roma Tor Vergata, Via della Ricerca Scientifica 1, 00133 Rome, Italy
and INFN, Sezione di Roma Tor Vergata, Via della Ricerca Scientifica 1, 00133 Rome, Italy

(Received 23 November 2020; revised 26 April 2021; accepted 20 May 2021; published 7 June 2021)

We show the formation of a nonequilibrium excitonic condensate in a bulk WSe_2 coherently pumped in resonance with the lowest-energy exciton. The lifetime of the superfluid is addressed by studying the screened dynamics during and after the pump pulse. Intervalley scattering causes electron migration from the optically populated K valley to the conduction band minimum at Σ. Due to the electron-hole imbalance at the K point a plasma of quasifree holes develops, which efficiently screens the interaction of the remaining excitons. We show that this plasma screening causes an ultrafast melting of the nonequilibrium condensate and that during melting coherent excitons and quasifree electron-hole pairs coexist. The time-resolved spectral function does exhibit a conduction and excitonic sidebands of opposite convexity and relative spectral weight that changes in time. Both the dependence of the time-dependent conduction density on the laser intensity and the time-resolved spectral function agree with recent ARPES experiments.

DOI: 10.1103/PhysRevB.103.L241404

Excitons in solids are electron-hole (e-h) bound pairs, which behave as composite bosons in the dilute limit [1–4]. More than three decades ago it was suggested that a nonequilibrium (NEQ) exciton superfluid may form in a semiconductor after pumping with coherent light of frequency smaller than the gap but larger than or at most equal to the exciton energy [5–8]. The pump would then drive the system from a nondegenerate ground state (insulating phase) to a symmetry-broken excited state known as the NEQ excitonic insulator (EI) [9–12]. Alternatively, the NEQ-EI state can be shown to emerge from the spontaneous symmetry breaking of a macroscopically degenerate excited manifold [12–21].

In time-resolved (tr) ARPES the NEQ-EI phase generates a replica of the valence band at the exciton energy, i.e., below the conduction band minimum (CBM) [5,12,22,23]. The experimental observation of this effect is challenging [24,25] since excitons may quickly lose coherence [26] due to electron-phonon scattering [27–30] or break into electron-hole pairs due to excited-state screening mechanisms [31–36]. As a result the ARPES signal changes rapidly with increasing pump-probe delay [22,23,37–39] and the measured spectra become difficult to interpret. The development of a microscopic theory, which takes into account decoherence, screening and other material-specific properties is therefore necessary in order to understand the ultrafast dynamics and interpret the experimental results.

In this work we put forward a microscopic theory for bulk WSe_2, an indirect gap semiconductor [40] with an optically bright exciton of energy slightly below the gap [41–45]. A distinct physical picture emerges from our calculations, see Fig. 1. The pump-induced photoexcitation initially generates an exciton superfluid around the K point [46,47]. Due to intervalley scattering [48], however, the bound electrons migrate from the K valley to the CBM at the Σ valley [40], causing the dissociation of excitons and hence the formation of a gas of free holes at the K point This hole-plasma efficiently screens [49–51] the electron-hole attraction and eventually causes an ultrafast melting of the remaining excitons [36]. During the melting process the quasifree e-h pairs coexist with excitons in the NEQ-EI phase.

Through real-time simulations and self-consistent excited-state calculations we show the formation of the NEQ-EI phase during resonant pumping as well as its fingerprints in tr-ARPES spectra. If screening is neglected then the excitonic sideband is simply attenuated by the K → Σ intervalley scattering as the pump-probe delay increases. If, instead, both screening and intervalley scattering are taken into account then the instantaneous formation of the excitonic sideband is followed by the development of a quasiparticle sideband,

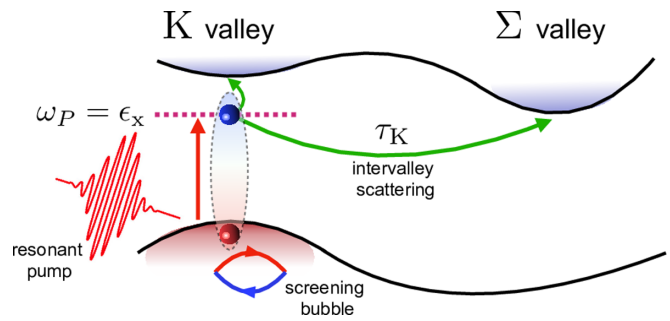

FIG. 1. The NEQ-EI state is created in the K valley, where bright excitons are initially photo-excited. Subsequent K → Σ intervalley scattering of excited carriers breaks charge neutrality in the K valley, and free K-valence holes screen the Coulomb repulsion. The reduction of e-h attraction causes exciton breaking, and free electrons occupy the available conduction states in the K valley.

signaling the coexistence of quasifree e-h pairs and excitons. The spectral weight is then rapidly transferred from the excitonic sideband to the quasiparticle sideband until the extinction of the former. The calculated tr-ARPES spectra of bulk WSe_2 agrees well with recent experiments on the same system [52] if the $K \to \Sigma$ scattering rate is estimated to be $\approx$15 fs [36,48,52]. Our simulations indicate that in this case the NEQ-EI phase melt in few tens of femtoseconds. Although the interplay of intervalley scattering and enhanced screening is investigated in bulk WSe_2 the highlighted mechanism is general and it is likely to occur in other indirect gap semiconductors.

In a bulk WSe_2 optical excitations of frequency close or below the direct gap at the K and K′ points [40] generate e-h pairs around the same points [46,47]. In the following we neglect the spin-orbit coupling and consider degenerate and decoupled K and K′ valleys. The inclusion of spin-orbit does not change the main conclusions. Recent first-principles calculations have shown that the band structure around the K valley has a strong two-dimensional (2D) character with negligible dispersion along the perpendicular direction [48] and with an (in-plane) effective mass almost identical to that of a monolayer [53].

Let $\epsilon_{v\mathbf{k}}$ and $\epsilon_{c\mathbf{k}}$ be the valence and conduction dispersion with $\mathbf{k}$ the 2D quasimomentum of a WSe_2 layer, and $\epsilon_g = 1.8$ eV [40–45] the direct gap. Placing the K point at $\mathbf{k} = 0$ we use quadratic dispersions $\epsilon_{v\mathbf{k}} = -\frac{k^2}{2m} - \frac{\epsilon_g}{2}$ and $\epsilon_{c\mathbf{k}} = \frac{k^2}{2m} + \frac{\epsilon_g}{2}$, with $k = |\mathbf{k}|$. We parametrize the bare electron-hole attraction $U_\mathbf{q}$ according to Ref. [38], yielding the lowest (bright) A exciton at energy $\epsilon_x = 1.7$ eV (binding energy $\epsilon_b = \epsilon_g - \epsilon_x = 0.1$ eV), in agreement with the literature [41,54].

We are interested in the electronic properties of WSe_2 under weak resonant pumping – hence with a photon frequency $\omega_P = \epsilon_x$. Pump-probe experiments [24,48,55,56] indicate that excited carriers experience a fast intervalley scattering due to electron-phonon interactions [29,57]. The intervalley scattering transfers the pumped electrons from the K valley to the CBM at the Σ valley on a time scale $\tau_K \approx 15$ fs [52]. At the Σ point the conduction states spread along the perpendicular direction [48] and electrons can escape from the WSe_2 layer. This leakage of conduction electrons is taken into account by adding a drain term to the equation of motion for the density matrix, see below.

Intervalley scattering has also a pivotal role in renormalizing the effective e-h attraction. The total conduction density $n_e(t)$ (i.e., the sum of K and K′ valleys contributions) becomes smaller than the corresponding valence hole density $n_h(t)$. This gives rise to a finite density $n_{pl} = (n_h - n_e)/2$ of free holes in each K valley. Under the weak pumping assumption the screening due to excitons is negligible and can be discarded [54,58]. Thus the screened e-h interaction $W_\mathbf{q}$ is

$$W_\mathbf{q} = \frac{U_\mathbf{q}}{1 - 2U_\mathbf{q}\chi^{\rm pl}_\mathbf{q}}, \tag{1}$$

with $\chi^{\rm pl}_\mathbf{q}$ the 2D Lindhard function [59]

$$\chi^{\rm pl}_\mathbf{q} = \frac{m}{\pi}\left[\theta(q - \sqrt{8\pi n_{\rm pl}})\sqrt{1 - \frac{8\pi n_{\rm pl}}{q^2}} - 1\right]. \tag{2}$$

With this premise, the equation of motion for the 2×2 one-particle density matrix $\rho_\mathbf{k} = \begin{pmatrix} \rho^{vv}_\mathbf{k} & \rho^{vc}_\mathbf{k} \\ \rho^{cv}_\mathbf{k} & \rho^{cc}_\mathbf{k} \end{pmatrix}$ in the Hartree plus screened exchange (HSEX) approximation reads

$$-i\frac{d}{dt}\rho_\mathbf{k}(t) + [h_{\rm HSEX,\mathbf{k}}(t), \rho_\mathbf{k}(t)] - \frac{i}{2}\{\gamma, \rho_\mathbf{k}(t)\} = 0, \tag{3}$$

where the 2×2 draining matrix $\gamma = \begin{pmatrix} 0 & 0 \\ 0 & \tau_K^{-1} \end{pmatrix}$ accounts for the intervalley scattering through an exponential depletion of the conduction density on the τ_K time scale. The explicit form of the time-dependent Hamiltonian $h_{\rm HSEX}$ in the presence of a pump pulse $E(t)$ coupled to the valence-conduction dipole moments $d_\mathbf{k}$ can be found in the Supplemental Material [54]. We emphasize that the HSEX potential depends on the density matrix explicitly as well as implicitly through the dependence of W on $n_{\rm pl} = (n_h - n_e)/2$. The density of conduction electrons and valence holes is indeed given by $n_e(t) = \frac{4}{\mathcal{N}\mathcal{A}}\sum_\mathbf{k}\rho^{cc}_\mathbf{k}(t)$ and $n_h(t) = \frac{4}{\mathcal{N}\mathcal{A}}\sum_\mathbf{k}[1 - \rho^{vv}_\mathbf{k}(t)]$, where $\mathcal{N}$ is the number of $\mathbf{k}$ points and $\mathcal{A} = 9.53 \times 10^{-16}$ cm^2 is the area of the unit cell of a WSe_2 layer. Here the factor of 4 in n_e and n_h accounts for the spin and valley degeneracy.

To gain insight on the nature of the time-dependent results we preliminarily discuss the Floquet solution of Eq. (3) for $\gamma = 0$ (no intervalley scattering and hence no screening). For this purpose we consider the solution of the BCS-like secular problem [12]

$$(h_{\rm HSEX,\mathbf{k}} - \mu)\varphi^\xi_\mathbf{k} = e^\xi_\mathbf{k}\varphi^\xi_\mathbf{k}, \tag{4}$$

where $\xi = \pm$ labels the two eigenvectors and $\mu = \begin{pmatrix} \mu_v & 0 \\ 0 & \mu_c \end{pmatrix}$ is a band-dependent chemical potential ensuring a finite density of e-h pairs. Equation (4) must be solved self-consistently since the HSEX potential is a functional of ρ, which, at zero temperature, can be written as [12,58] $\rho^{\alpha\beta}_\mathbf{k} = \varphi^-_{\alpha\mathbf{k}}\varphi^{-*}_{\beta\mathbf{k}}$. Symmetry broken, i.e., $\rho^{cv}_\mathbf{k} \neq 0$, NEQ-EI solutions exist if the difference between the chemical potentials is larger than the lowest exciton energy ϵ_x, i.e., $\delta\mu \equiv \mu_c - \mu_v > \epsilon_x$ [12]. They have infinite degeneracy since if $\varphi^\xi_\mathbf{k} = \begin{pmatrix} \varphi^\xi_{v\mathbf{k}} \\ \varphi^\xi_{c\mathbf{k}} \end{pmatrix}$ is a solution then $\varphi^\xi_\mathbf{k}(\theta) = \begin{pmatrix} \varphi^\xi_{v\mathbf{k}} \\ e^{i\theta}\varphi^\xi_{c\mathbf{k}} \end{pmatrix}$ is a solution too. In the dilute limit the total number of zero-momentum excitons $N_{\rm ex}$ is equal to the total number of excited electrons N_e in the conduction bands [54], i.e.,

$$N_{\rm ex} = N_e. \tag{5}$$

Thus all e-h pairs are bound excitons condensed in the lowest-energy state. In Fig. 2 we show the values of the excitonic order parameter $\Delta = -\frac{1}{\mathcal{N}}\sum_\mathbf{q} W_\mathbf{q}\rho^{vc}_\mathbf{q}$ for the two-band model of WSe_2; Δ is nonvanishing up to high densities $n_e \sim 10^{13}$cm^{-2}, and it reaches its maximum value for $n_e \sim 5 \times 10^{11}$cm^{-2}. Using the NEQ-EI symmetry-broken density matrix as initial condition the Floquet state

$$\rho_\mathbf{k}(t) = e^{i\sigma_z\frac{\delta\mu}{2}t}\rho_\mathbf{k}(0)e^{-i\sigma_z\frac{\delta\mu}{2}t} \tag{6}$$

is a solution of Eq. (3) for $\gamma = 0$ [23]. This state is characterized by persistent monochromatic oscillations of the order parameter, $\Delta(t) = e^{i\delta\mu t}\Delta(0)$, and the corresponding ARPES signal displays a replica of the valence band (shifted upward by ϵ_x) inside the gap, see inset of Fig. 2. Moreover the spectral

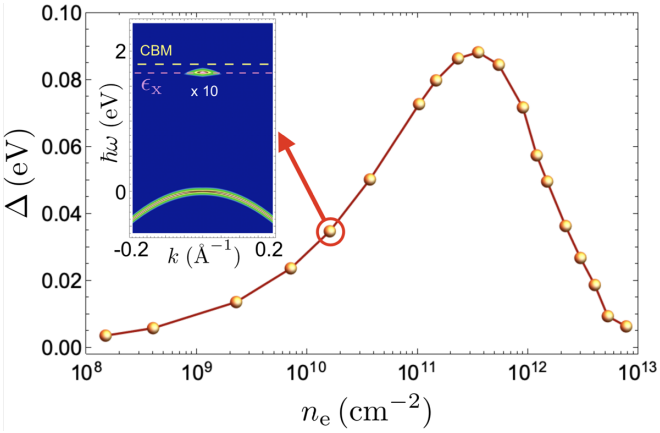

FIG. 2. Excitonic order parameter Δ versus excitation density n_e. The inset shows the spectral function [54] for $n_e = 1.6 \times 10^{10}\text{cm}^{-2}$. The excitonic sideband has been magnified by a factor 10 for a better visualization. Energies are measured with respect to the maximum of the valence band (VBM). Horizontal dashed lines at $\omega = \epsilon_g$ and $\omega = \epsilon_x$ are also drawn.

weight of the excitonic sideband is proportional to the square of the excitonic wave function.

We now show that the NEQ-EI (Floquet) phase can be generated in real time by driving the system with laser pulses resonant with the exciton energy. The inclusion of intervalley scattering ($\gamma \neq 0$) and screening, however, affects the stability of the photoinduced exciton superfluid, with inevitable and interesting repercussions on the time dependence of the ARPES spectrum. We solve Eq. (3) numerically with the ground-state density matrix $\rho_{g,\mathbf{k}} = \left(\begin{smallmatrix} 1 & 0 \\ 0 & 0 \end{smallmatrix}\right)$ as initial condition. In the simulations the system is excited by a visible pump pulse $E(t)$ of finite duration T_P, maximum intensity E_P and resonant frequency $\omega_P = \epsilon_x$. To display the numerical results we set the origin of times at $T_P/2$ (pump peak). This choice is motivated by the experimental convention of setting the origin of the pump-probe delays τ at the coincidence between the pump and probe peaks. Our time origin then allows for a direct comparison with experiments since the conduction density $\rho^{cc}_{\mathbf{k}}(\tau)$ at time τ is proportional to the time-resolved (tr) ARPES weight at quasimomentum $\mathbf{k}$ and pump-probe delay τ [54]. We assume momentum-independent dipole moments $d_{\mathbf{k}} = d$ and define the Rabi frequency, which determines the strength of the light-matter coupling, as $\Omega_P = E_P d$. The simulations have been performed with the CHEERS code [60] using pumps of duration $T_P = 100$ fs (FWHM = 50 fs). According to our convention the initial time is then $t = -50$ fs. We calculate the density of conduction electrons $n_e(t)$ and valence holes $n_h(t)$ as well as the time-dependent order parameter $\Delta(t) = -\frac{1}{\mathcal{N}} \sum_{\mathbf{q}} W_{\mathbf{q}} \rho^{vc}_{\mathbf{q}}(t)$. We also calculate the time-dependent spectral function $A_{\mathbf{k}}(\tau, \omega)$ at time τ using a probing temporal window of $T_p = 70$ fs [54]. This quantity is proportional to the tr-ARPES spectrum measured by a extreme ultraviolet probe of duration T_p at delay τ [23].

In Fig. 3 we show $n_e(t)$ for different relative intensities $I_r = (\Omega_P/\Omega_0)^2$, with $\Omega_0 = 13$ meV. The time at which $n_e(t)$ is maximum approaches zero with increasing intensity, in agreement with the experimental evidence reported in Ref. [52].

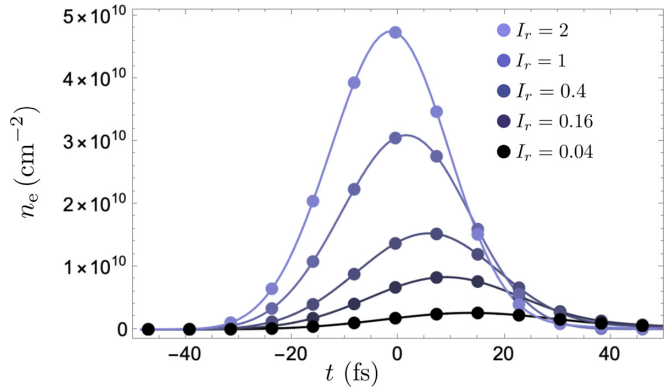

FIG. 3. Temporal evolution of the excited density $n_e(t)$ for different pump intensities I_r.

This corroborates the validity of the time-dependent plasma screening approximation in Eqs. (1) and (2). In fact, the maximum of $n_e(t)$ is independent of I_r in simulations with an unscreened interaction (not shown).

In Fig. 4 we show n_e (red) and n_{pl} (blue) in Fig. 4(a) as well as the order parameter Δ in Fig. 4(b) for $\Omega_P = 13$ meV. During photoexcitation the order parameter $\Delta(t)$ starts oscillating, signaling the creation of a coherent exciton superfluid. For $t \lesssim -25$ fs the effects of intervalley scattering are negligible, and the plasma density remains small. According to Eqs. (1) and (2) screening is weak and the dynamics is close to the unscreened one. In this early transient stage the system visits instantaneously all NEQ-EI states belonging to the phase diagram of Fig. 2 [54]. In fact, a weak resonant photoexcitation can only create coherent excitons (quasiparticle states are accessible only for $\omega_P > \epsilon_g$) and hence $N_e(t) = N_{ex}(t)$. The situation changes when electrons start migrating toward the Σ valley. As the K valley is depleted the plasma density n_{pl} grows, see Fig. 4(a), and hence the effective electron-hole attraction becomes weaker; as a consequence the order parameter starts decaying, see Fig. 4(b). At $t \approx 35$–40 fs no excited carriers remain in the K valley. To shed light on the physical scenario in this stage we calculate the transient spectral function [54]. In Fig. 5 we show $A_{\mathbf{k}}(\tau, \omega)$ at different delays τ. For $\tau \lesssim 0$ the spectral function exhibits the typical feature of the

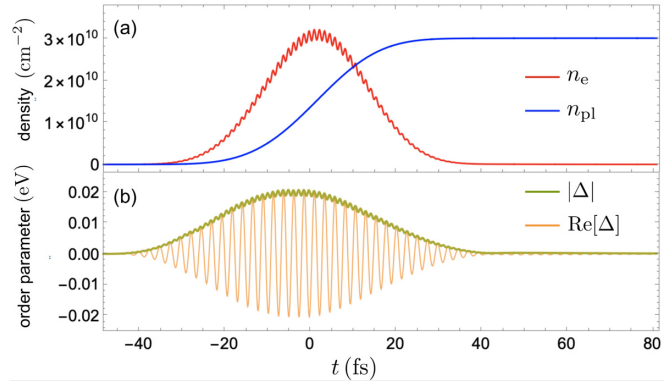

FIG. 4. Temporal evolution of (a) the excited density $n_e(t)$ (red curve) and screening density $n_{pl}(t)$ (blue curve), and (b) order parameter $\Delta(t)$.

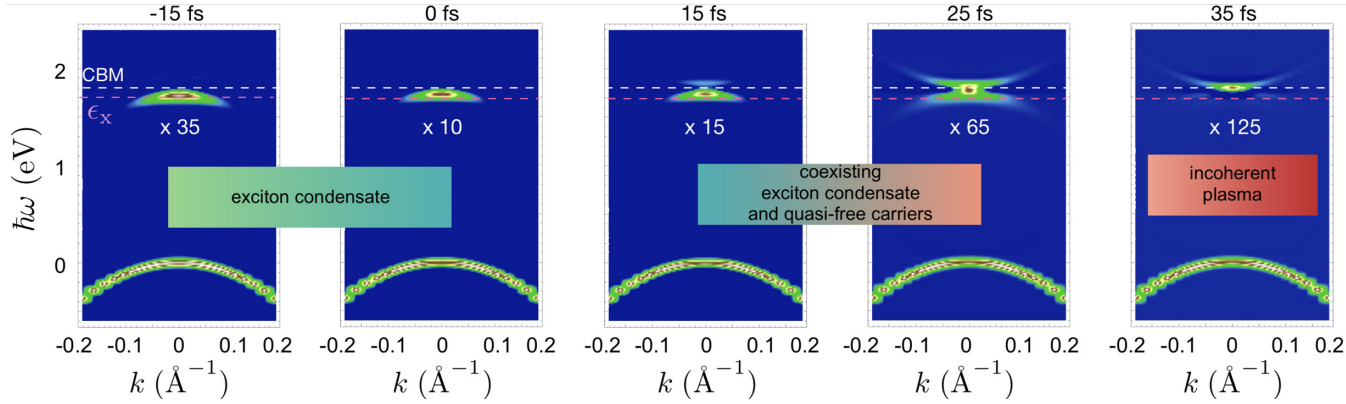

FIG. 5. Transient spectral function $A_{\mathbf{k}}(\tau,\omega)$ at different delays. The intensity from the conduction band is multiplied by the factor $M = S_v/S_c$ where S_α is the spectral weight of band $\alpha = v, c$ at $\mathbf{k} = 0$. Energies are measured with respect to the valence band maximum. Horizontal dashed lines at energies ϵ_g (white) and ϵ_x (red) are drawn to guide the eye.

NEQ-EI phase, i.e., an excitonic replica of the valence band at energy $\epsilon_x < \epsilon_g$. At these delays the unscreened and screened spectral functions are almost identical since $n_{\rm pl} \simeq 0$ [54]. At delays $\tau \gtrsim 15$ fs a spectral structure right above the CBM emerges. Therefore excitons start breaking into e-h pairs and the freed electrons settle down in the empty levels around the CBM; in this time window excitons in the NEQ-EI phase and a plasma of free carriers coexist. As time increases the number of bound e-h pairs at the K point becomes smaller and eventually the spectral weight is totally transferred to the conduction band. At delays $\tau \gtrsim 35$ fs only the conduction band is visible, implying that all carriers are free. This incoherent regime lasts until the migration from K to Σ is completed, i.e., until $\tau \approx 40$ fs. It is worth noting that if screening is neglected [hence $W_{\mathbf{q}}(t) = U_{\mathbf{q}}$ but $\gamma \neq 0$] then the spectral structure around the CMB does not emerge [54]. This implies that conduction electrons at K remain bound and excitons break only into free electrons at Σ and free holes at K. According to this scenario it is reasonable to expect that in direct gap systems such as, e.g., WSe_2 monolayer, where the intervalley scattering is not relevant, the excitonic sideband survives for longer times.

As anticipated, in the dilute limit the intensity of the excitonic sideband is proportional to the exciton wave function $Y_{\mathbf{k}}$. In particular, for a delay τ at which the system is in a pure NEQ-EI, we have [54]

$$|Y_{\mathbf{k}}|^2 \propto \mathcal{I}_{\mathbf{k}} = \int d\omega A_{\mathbf{k}}(\tau,\omega), \tag{7}$$

where the integral is performed over a frequency domain that excludes the valence band (in our case $1\,\text{eV} \lesssim \omega \lesssim 3\,\text{eV}$ in Fig. 5). In Fig. 6 we show the comparison between $|Y_{\mathbf{k}}|^2$ and $\mathcal{I}_{\mathbf{k}}$ for two different pump fluences. In the linear response regime ($I_r = 0.04$) the agreement is excellent, whereas for the higher fluence $I_r = 1$ used in Fig. 5 the curve $\mathcal{I}_{\mathbf{k}}$ displays a suppression of the k derivative at $k = 0$, signaling a departure form the linear response regime.

To summarize, we have studied the screened dynamics of the excitonic condensate forming in a bulk WSe_2 upon pumping in resonance with the lowest-energy bright exciton. We have shown how in the low-density regime the tr-ARPES spectrum can be used for an accurate measurement of the exciton wave function. Through the transient spectral function we have been also able to observe the transition from an initial NEQ-EI phase of coherent excitons to a final phase of incoherent e-h pairs. This transition is not abrupt as the two phases coexist. The proposed theory relies on a general mechanism based on the interplay between intervalley scattering and plasma screening and the results agree with recent findings on the same system [52]. In fact, neglecting the renormalization of the effective e-h attraction the excitons at the K point would not break into e-h pairs at the same point and hence no signal from the conduction band would be detected at K. Furthermore, the delay τ at which the maximum value of the conduction density occurs would be independent of the intensity of the pump pulse.

The screening due to quasifree holes arising from the intervalley scattering is responsible for an ultrafast melting of the NEQ-EI phase. Although this mechanism has been highlighted in WSe_2 it is likely to occur in other indirect gap semiconductors as the only condition to meet is that electrons migrating from a local valley of the conduction band to the global CBM do not bounce back. The results presented in this work are based on a 2D two-band model. However, the

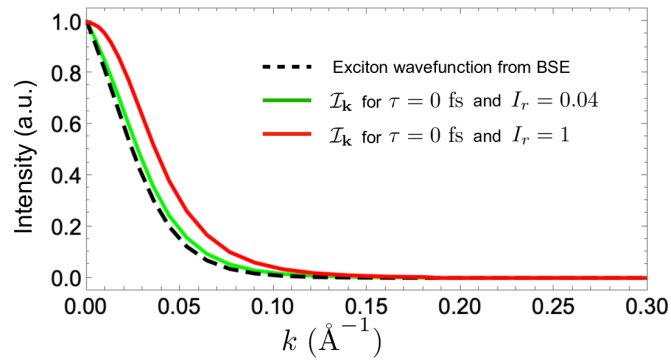

FIG. 6. Square modulus of the exciton wave function $|Y_{\mathbf{k}}|^2$ obtained from the solution of the Bethe-Salpeter equation [54] (black dashed line) and the intensity the excitonic sideband $\mathcal{I}_{\mathbf{k}}$ extracted from the transient spectral function at $\tau = 0$ fs for two different pump fluences $I_r = 0.04$ (green line) and $I_r = 1$ (red line). All quantities are normalized to their maximum value.

underlying theory is general and the adiabatic screening of the effective nonequilibrium e-h interaction makes it suitable for implementations in available first-principles codes [61], thus providing a route to account explicitly for the spin-orbit interaction, the Σ valley degrees of freedom as well as the phonon-induced intervalley scattering.

We acknowledge useful discussions with Andrea Marini and Davide Sangalli. We also acknowledge funding from MIUR PRIN Grant No. 20173B72NB and from INFN20-TIME2QUEST project. G.S. acknowledges Tor Vergata University for financial support through the Beyond Borders Project ULEXIEX.

[1] L. Keldysh, *Problems of Theoretical Physics* (Oxford Academic, Oxford, 1972).
[2] L. V. Keldysh and A. N. Kozlov, JETP **27**, 521 (1968).
[3] S. A. Moskalenko and D. W. Snoke, *Bose-Einstein Condensation of Excitons and Biexcitons* (Cambridge University Press, Cambridge, 2000).
[4] M. Combescot and S. Shiau, *Excitons and Cooper Pairs: Two Composite Bosons in Many-body Physics*, Oxford graduate texts (Oxford University Press, Oxford, 2016).
[5] S. Schmitt-Rink, D. S. Chemla, and H. Haug, Phys. Rev. B **37**, 941 (1988).
[6] J. R. Kuklinski and S. Mukamel, Phys. Rev. B **42**, 2959 (1990).
[7] S. Glutsch and R. Zimmermann, Phys. Rev. B **45**, 5857 (1992).
[8] P. Littlewood and X. Zhu, Phys. Scr. **1996**, 56 (1996).
[9] T. Östreich and K. Schönhammer, Z. Phys. B **91**, 189 (1993).
[10] K. Hannewald, S. Glutsch, and F. Bechstedt, J. Phys.: Condens. Matter **13**, 275 (2000).
[11] S. Glutsch, F. Bechstedt, and R. Zimmermann, Phys. Status Solidi B **172**, 357 (1992).
[12] E. Perfetto, D. Sangalli, A. Marini, and G. Stefanucci, Phys. Rev. Mater. **3**, 124601 (2019).
[13] M. H. Szymańska, J. Keeling, and P. B. Littlewood, Phys. Rev. Lett. **96**, 230602 (2006).
[14] R. Hanai, P. B. Littlewood, and Y. Ohashi, J. Low Temp. Phys. **183**, 127 (2016).
[15] R. Hanai, P. B. Littlewood, and Y. Ohashi, Phys. Rev. B **96**, 125206 (2017).
[16] C. Triola, A. Pertsova, R. S. Markiewicz, and A. V. Balatsky, Phys. Rev. B **95**, 205410 (2017).
[17] R. Hanai, P. B. Littlewood, and Y. Ohashi, Phys. Rev. B **97**, 245302 (2018).
[18] A. Pertsova and A. V. Balatsky, Phys. Rev. B **97**, 075109 (2018).
[19] K. W. Becker, H. Fehske, and V.-N. Phan, Phys. Rev. B **99**, 035304 (2019).
[20] M. Yamaguchi, K. Kamide, R. Nii, T. Ogawa, and Y. Yamamoto, Phys. Rev. Lett. **111**, 026404 (2013).
[21] A. Pertsova and A. V. Balatsky, Ann. Phys. (NY) **532**, 1900549 (2020).
[22] D. Christiansen, M. Selig, E. Malic, R. Ernstorfer, and A. Knorr, Phys. Rev. B **100**, 205401 (2019).
[23] E. Perfetto, S. Bianchi, and G. Stefanucci, Phys. Rev. B **101**, 041201(R) (2020).
[24] J. Madéo, M. K. Man, C. Sahoo, M. Campbell, V. Pareek, E. L. Wong, A. A. Mahboob, N. S. Chan, A. Karmakar, B. M. K. Mariserla *et al.*, Science, **370**, 1199 (2020).
[25] W. Lee, Y. Lin, L.-S. Lu, W.-C. Chueh, M. Liu, X. Li, W.-H. Chang, R. A. Kaindl, and C.-K. Shih, arXiv:2008.06103.
[26] S. W. Koch, M. Kira, G. Khitrova, and H. M. Gibbs, Nature Mater. **5**, 523 (2006).
[27] A. B. Madrid, K. Hyeon-Deuk, B. F. Habenicht, and O. V. Prezhdo, ACS nano **3**, 2487 (2009).
[28] Z. Nie, R. Long, L. Sun, C.-C. Huang, J. Zhang, Q. Xiong, D. W. Hewak, Z. Shen, O. V. Prezhdo, and Z.-H. Loh, ACS Nano **8**, 10931 (2014).
[29] M. Selig, G. Berghäuser, A. Raja, P. Nagler, C. Schüller, T. F. Heinz, T. Korn, A. Chernikov, E. Malic, and A. Knorr, Nature Commun. **7**, 13279 (2016).
[30] D. Sangalli, E. Perfetto, G. Stefanucci, and A. Marini, Eur. Phys. J. B **91**, 171 (2018).
[31] A. Chernikov, A. M. van der Zande, H. M. Hill, A. F. Rigosi, A. Velauthapillai, J. Hone, and T. F. Heinz, Phys. Rev. Lett. **115**, 126802 (2015).
[32] A. Chernikov, C. Ruppert, H. M. Hill, A. F. Rigosi, and T. F. Heinz, Nature Photon. **9**, 466 (2015).
[33] P. D. Cunningham, A. T. Hanbicki, K. M. McCreary, and B. T. Jonker, ACS Nano **11**, 12601 (2017).
[34] K. Yao, A. Yan, S. Kahn, A. Suslu, Y. Liang, E. S. Barnard, S. Tongay, A. Zettl, N. J. Borys, and P. J. Schuck, Phys. Rev. Lett. **119**, 087401 (2017).
[35] J. Wang, J. Ardelean, Y. Bai, A. Steinhoff, M. Florian, F. Jahnke, X. Xu, M. Kira, J. Hone, and X.-Y. Zhu, Sci. Adv. **5**, eaax0145 (2019).
[36] M. Dendzik, R. P. Xian, E. Perfetto, D. Sangalli, D. Kutnyakhov, S. Dong, S. Beaulieu, T. Pincelli, F. Pressacco, D. Curcio *et al.*, Phys. Rev. Lett. **125**, 096401 (2020).
[37] E. Perfetto, D. Sangalli, A. Marini, and G. Stefanucci, Phys. Rev. B **94**, 245303 (2016).
[38] A. Steinhoff, M. Florian, M. Rösner, G. Schönhoff, T. O. Wehling, and F. Jahnke, Nature Commun. **8**, 1166 (2017).
[39] A. Rustagi and A. F. Kemper, Phys. Rev. B **97**, 235310 (2018).
[40] H. Jiang, J. Phys. Chem. C **116**, 7664 (2012).
[41] A. Beal and W. Liang, J. Phys. C: Solid State Phys. **9**, 2459 (1976).
[42] T. Finteis, M. Hengsberger, T. Straub, K. Fauth, R. Claessen, P. Auer, P. Steiner, S. Hüfner, P. Blaha, M. Vögt *et al.*, Phys. Rev. B **55**, 10400 (1997).
[43] A. Arora, M. Koperski, K. Nogajewski, J. Marcus, C. Faugeras, and M. Potemski, Nanoscale **7**, 10421 (2015).
[44] J. M. Riley, W. Meevasana, L. Bawden, M. Asakawa, T. Takayama, T. Eknapakul, T. Kim, M. Hoesch, S.-K. Mo, H. Takagi *et al.*, Nature Nanotech. **10**, 1043 (2015).
[45] B. S. Kim, J.-W. Rhim, B. Kim, C. Kim, and S. R. Park, Sci. Rep. **6**, 36389 (2016).
[46] R. Frindt, J. Phys. Chem. Solids **24**, 1107 (1963).
[47] G. Wang, A. Chernikov, M. M. Glazov, T. F. Heinz, X. Marie, T. Amand, and B. Urbaszek, Rev. Mod. Phys. **90**, 021001 (2018).

[48] R. Bertoni, C. W. Nicholson, L. Waldecker, H. Hübener, C. Monney, U. De Giovannini, M. Puppin, M. Hoesch, E. Springate, R. T. Chapman *et al.*, Phys. Rev. Lett. **117**, 277201 (2016).
[49] A. Steinhoff, M. Rösner, F. Jahnke, T. O. Wehling, and C. Gies, Nano Lett. **14**, 3743 (2014).
[50] Y. Liang and L. Yang, Phys. Rev. Lett. **114**, 063001 (2015).
[51] L. Meckbach, T. Stroucken, and S. W. Koch, Appl. Phys. Lett. **112**, 061104 (2018).
[52] M. Puppin, Freie Universität Berlin, Ph. D. thesis, 2018, http://dx.doi.org/10.17169/refubium-804.
[53] H. Peelaers and C. G. Van de Walle, Phys. Rev. B **86**, 241401(R) (2012).
[54] See Supplemental Material http://link.aps.org/supplemental/10.1103/PhysRevB.103.L241404 for details on the microscopic model, the Floquet solution of Eq. (3), proof of Eq. (5), time-dependent simulations in the unscreened case, and explicit evaluation of the transient spectral function. The Supplemental Material also includes Refs. [62–80].
[55] R. Wallauer, J. Reimann, N. Armbrust, J. Güdde, and U. Höfer, Appl. Phys. Lett. **109**, 162102 (2016).
[56] L. Waldecker, R. Bertoni, H. Hübener, T. Brumme, T. Vasileiadis, D. Zahn, A. Rubio, and R. Ernstorfer, Phys. Rev. Lett. **119**, 036803 (2017).
[57] A. Molina-Sánchez, D. Sangalli, L. Wirtz, and A. Marini, Nano Lett. **17**, 4549 (2017).
[58] E. Perfetto, A. Marini, and G. Stefanucci, Phys. Rev. B **102**, 085203 (2020).
[59] G. Giuliani and G. Vignale, *Quantum Theory of the Electron Liquid* (Cambridge University Press, Cambridge, 2005).
[60] E. Perfetto and G. Stefanucci, J. Phys.: Condens. Matter **30**, 465901 (2018).
[61] D. Sangalli, A. Ferretti, H. Miranda, C. Attaccalite, I. Marri, E. Cannuccia, P. Melo, M. Marsili, F. Paleari, A. Marrazzo *et al.*, J. Phys.: Condens. Matter **31**, 325902 (2019).
[62] R. E. Groenewald, M. Rösner, G. Schönhoff, S. Haas, and T. O. Wehling, Phys. Rev. B **93**, 205145 (2016).
[63] J. M. Blatt, K. W. Bö er, and W. Brandt, Phys. Rev. **126**, 1691 (1962).
[64] L. V. Keldysh and Y. U. Kopaev, Sov. Phys. Solid State **6**, 2219 (1965).
[65] Y. Wakisaka, T. Sudayama, K. Takubo, T. Mizokawa, M. Arita, H. Namatame, M. Taniguchi, N. Katayama, M. Nohara, and H. Takagi, Phys. Rev. Lett. **103**, 026402 (2009).
[66] K. Sugimoto, S. Nishimoto, T. Kaneko, and Y. Ohta, Phys. Rev. Lett. **120**, 247602 (2018).
[67] H. Cercellier, C. Monney, F. Clerc, C. Battaglia, L. Despont, M. G. Garnier, H. Beck, P. Aebi, L. Patthey, H. Berger, and L. Forró, Phys. Rev. Lett. **99**, 146403 (2007).
[68] A. Kogar, M. S. Rak, S. Vig, A. A. Husain, F. Flicker, Y. I. Joe, L. Venema, G. J. Mac-Dougall, T. C. Chiang, E. Fradkin, J. van Wezel, and P. Abbamonte, Science **358**, 1314 (2017).
[69] D. Varsano, S. Sorella, D. Sangalli, M. Bar-borini, S. Corni, E. Molinari, and M. Rontani, Nature Commun. **8**, 1461 (2017).
[70] M. M. Fogler, L. V. Butov, and K. S. Novoselov, Nature Commun. **5**, 4555 (2014).
[71] J. I. A. Li, T. Taniguchi, K. Watanabe, J. Hone, and C. R. Dean, Nature Phys. **13**, 751 (2017).
[72] L. Du, X. Li, W. Lou, G. Sullivan, K. Chang, J. Kono, and R.-R. Du, Nature Commun. **8**, 1971 (2017).
[73] F.-C. Wu, F. Xue, and A. H. MacDonald, Phys. Rev. B **92**, 165121 (2015).
[74] D. Varsano, M. Palummo, E. Molinari, and M. Rontani, Nature Nanotechnol. **15**, 367 (2020).
[75] E. Perfetto and G. Stefanucci, Phys. Rev. Lett. **125**, 106401 (2020).
[76] J. K. Freericks, H. R. Krishnamurthy, and T. Pruschke, Phys. Rev. Lett. **102**, 136401 (2009).
[77] G. Stefanucci and R. van Leeuwen, *Nonequilibrium Many-Body Theory of Quantum Systems: A Modern Introduction* (Cambridge University Press, Cambridge, 2013).
[78] P. Lipavský, V. Špička, and B. Velický, Phys. Rev. B **34**, 6933 (1986).
[79] E. Perfetto, A.-M. Uimonen, R. van Leeuwen, and G. Stefanucci, Phys. Rev. A **92**, 033419 (2015).
[80] S. Latini, E. Perfetto, A.-M. Uimonen, R. van Leeuwen, and G. Stefanucci, Phys. Rev. B **89**, 075306 (2014),